Understanding the Electronic Structure, Reactivity, and Hydrogen Bonding for a 1,2-Diphosphonium Dication

David J. Wolstenholme,*,† Jan J. Weigand,‡ Reagan J. Davidson,† Jason K. Pearson,† and T. Stanley Cameron†

Department of Chemistry, Dalhousie University, Halifax, Nova Scotia, Canada, B3H 4J3, and Westfälische Wilhelms-Universität Münster, Institut für Anorganische und Analytische Chemie, Corrensstrasse 28/30, D-48149 Münster, Germany

Received: November 1, 2007; In Final Form: January 14, 2008

The experimental charge density for hexamethyldiphosphonium ditriflate has been determined from low-temperature high-resolution X-ray diffraction data. These results have been compared with theoretically calculated values for the isolated gas-phase compound. Analysis of the topological and atomic basin properties has provided insight into the exact nature of the P−P bond in both the crystalline and the gas-phase structures. The $\rho_b(\mathbf{r})$ and $\nabla^2\rho_b(\mathbf{r})$ values highlight the covalent nature of the P−P bond, while the atomic charges indicate a localization of the positive charges on the two phosphorus atoms. This seems to indicate that a covalent bond is formed despite a strong electrostatic repulsion between these two heteroatoms. The topological properties and electrostatic potentials have also been shown to provide significant insight into the chemical reactivity of the title compound. A topological analysis of P_2Me_4, $P_2Me_5^+$, and $P_2Me_6^{+2}$ species has provided information about the progression of the P−P bond in the synthesis of the title compound. An investigation of the different hydrogen-bonding networks present in the crystalline and gas-phase structures, along with their affect on the electronic structure of the title compound has also been investigated. This has all led to significant new insight into the electronic structure, reactivity, and weak hydrogen bonding in prototypical 1,2-diphosphonium dications.

Introduction

The investigation of molecules that possess unusual chemical bonding comprises one of the most fascinating topics in modern day chemistry. Such studies push the limits of our traditional views of chemical bonding and can provide a better understanding of complex chemical phenomena. One such example is the examination of the electronic structure of 1,2-dications. These molecules possess an interesting E^+-E^+ (E = C, N, S, P, etc...) framework, which can show remarkable chemical stability, despite the expected strong electrostatic repulsion experienced by the two heteroatoms. In particular, the study of diphosphonium dications has received considerable interest, as a result of the diagonal relationship between carbon and phosphorus.[1,2]

In the early literature, structurally characterized compounds containing a P^+-P^+ unit were stabilized through the use of sterically bulky amine substituents or polycyclic frameworks.[3−6] However, a recent study[2] has shown that alkylation reactions of either diphosphines or phosphinophosphonium cations with the powerful alkylating agent methyltriflate leads to the isolation of a series of symmetric, homoleptic nonsymmetric and heteroleptic symmetric hexaalkylated 1,2-diphosphonium derivatives as bottleable salts in high yields. This class of compounds represents prototypical phosphorus analogues of ethane, and the reported derivatives have been thoroughly investigated through spectroscopic and diffraction techniques.[2] This result is unexpected, since a chemical bond between two atoms bearing like charges should destabilize the molecule and without further stabilization should not exist. In these compounds, the phosphorus atoms are highly electrophilic; hence, 1,2-diphosphonium salts would be expected to be highly reactive and therefore represent interesting reagents for fundamental chemical transformations. Theoretically, the stability and reactivity of 1,2-diphosphonium dications have been estimated by means of quantum-chemical methods;[7] however, a detailed investigation of the electron distribution in such 1,2-diphosphonium dications has not until now been undertaken.

The quantum theory of atoms in molecules (QTAIM) extracts information on chemical bonding from the experimental and theoretical topologies of the electron density.[8,9] This provides a means of evaluating the exact nature of a chemical bond based on the properties of the electron density rather than being limited to a characterization based on geometrical features alone. This is achieved by locating a bond path and a bond critical point (BCP) for any chemical interaction of interest. A bond path represents a line in space linking two chemically bonded atoms, in which the electron density is a maximum with respect to any neighboring line of electron density. A rational bond path can be considered as a universal indicator of bonding regardless of its nature.[8] The BCP represents a minimum in the electron density along the bond path but a maximum in the two principal directions perpendicular to the tangent of the bond path at the BCP. This special point can be considered a gateway between two bonded atoms.

In this paper, we provide the first topological analysis of a 1,2-diphosphonium dication (hexamethyldiphosphonium ditriflate, Scheme 1), with particular emphasis on the adjacent positively charged P−P bond. The classification of the P−P bond

* To whom correspondence should be addressed. Phone: +1-(902)-494-3759. E-mail: dwolsten@dal.ca.
† Dalhousie University.
‡ Westfälische Wilhelms-Universität Münster.

10.1021/jp710527z CCC: $40.75
Published on Web 03/19/2008

SCHEME 1: Structural Diagram of the Hexamethyldiphosphonium Ditriflate

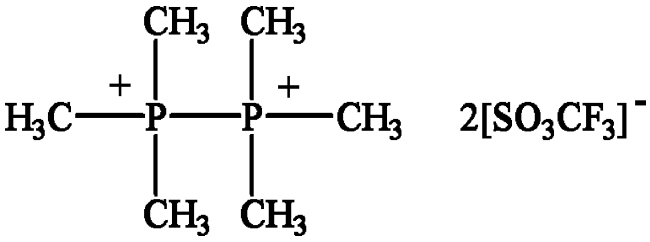

is based on various criteria obtained from the results of the multipole refinement of high-resolution X-ray data. This includes the accumulation of electron density [$\rho_b(\mathbf{r})$], the Laplacian [$\nabla^2\rho_b(\mathbf{r})$], and the length of the interaction line [R_{ij}]. Furthermore, we have investigated the electrostatic and atomic basin properties associated with this compound to provide better insight into the nature of the P^+-P^+ bond and its reactivity. This is followed by a comparison with the theoretically calculated electron density obtained from the analogous gas-phase compound. The isolated gas-phase species of P_2Me_4, $P_2Me_5^+$, and $P_2Me_6^{+2}$ have also been investigated theoretically, in order to show the progression of the P−P bond topological properties from the neutral species to the dication.

Experimental Measurement and Data Refinement

A needle-shaped, colorless crystal of hexamethyldiphosphonium ditriflate was mounted on the end of a MicroMount. This is essentially a tube of polyimide (used in Kapton tape) cut away to provide a nib-like shape with a loop at the top where the crystal is mounted. This tube has a greater resistance to vibration than a fiber of the same cross section. Single crystal, high-resolution X-ray diffraction data were collected on a Rigaku RAPID diffractometer using a sealed Mo−Kα radiation source. A summary of the crystal data from the diffraction experiment can be found in Table 1. The data were collected at a temperature of 123 ± 1 K to a maximum 2θ value of 144.8°, using overlapping frames. The data was processed with d*TREK as included in the CrystalClear software package.[11] The crystal structure was then solved by direct methods and expanded using Fourier techniques using the CrystalStructure software package.[12] Further details for the data collection are available in Supporting Information.

In the multipole refinement, 1405 unique reflections [$\sin\theta/\lambda = 1.078$ Å^{-1}] with $I > 3\sigma(I)$ were employed according to the Hansen−Coppens formalism.[13] The multipole refinement was carried out with the module XDLSM incorporated in the software package XD2006.[14] The scattering factors used throughout this refinement were those derived from Su, Macchi, and Coppens wave functions for all atoms.[15,16] The multipole expansion was applied up to the hexadecapole level ($l_{max} = 4$) for all heavy atoms and up to the dipole level ($l_{max} = 1$) for the hydrogen atoms. Separate κ and κ' parameters were employed for all heavy atoms throughout the multipole refinement. The expansion/contraction parameters for the hydrogen atoms were left fixed at the default XDLSM value of 1.2. The phosphorus and sulfur atoms were also refined using third-order Gram-Charlier expansion coefficients in order to significantly improve the R factor and residual features of the electron density. The C−H bond lengths were then set to the reported neutron diffraction distances of similar compounds (C−H = 1.059).[17] The 3m local site symmetry was applied to the multipole and thermal parameters for the S1, P1, and C1 atoms, while mirror plane symmetry was applied to the F1, O1, C2, and H1 atoms.[14]

TABLE 1: Experimental X-ray Data

compound formula	$P_2(CH_3)_6$, $2(SO_3CF_3)$
temperature (K)	123.0(1)
crystal size (mm)	0.12 × 0.23 × 0.27
crystal shape	needle
crystal color	colorless
wavelength	0.7107
space group	R-3m
formula weight (g/mol)	450.28
a/b (Å)	9.1795(4)
c (Å)	17.7956(10)
γ (°)	120.00
V (Å^3)	1298.62(11)
Z	3
μ (cm^{-1})	0.576
D_c (g/cm^3)	1.727
F (000)	690
max 2θ (collected)	144.8
sin θ/λ	1.078
reflections total	14014
reflections (multipole)	1405
$R(F)$	2.14
$R_w(F)$	2.84
GOF (multipole)	1.126
collection range	$-24 \le h \le 23$
	$-20 \le k \le 13$
	$-44 \le l \le 44$

The following strategy was cycled through until convergence was achieved: (a) a high-order ($\sin\theta/\lambda \ge 0.6$) refinement of the heavy atoms, (b) a low-order ($\sin\theta/\lambda \le 0.6$) refinement of the hydrogen atoms, (c) P_{lm}, (d) P_v, (e) κ and κ' for all heavy atoms, and (f) positional and thermal parameters for all heavy atoms. The difference mean square displacement amplitudes (DMSDA) for all bonds were within the Hirshfeld limits, which showed that the thermal motion had been successfully deconvoluted from the electron deformation caused by bonding and hybridization. The XDPROP and TOPXD programs incorporated into the XD2006 software[14] were then used to determine topological and atomic basin properties for the experimental electron density. All two-dimensional static, residual, dynamic, and deformation maps were produced using the XDGRAPH option in the XD2006 package.[14] The three-dimensional electrostatic potential maps were produced using the graphical program Molekel.[18]

Computational Methods

An unconstrained geometry optimization of the hexamethyldiphosphonium ditriflate compound was performed at the (DFT)-B3LYP/6-31++G(d,p) level of theory starting from the experimental geometry. The isolated P_2Me_4, $P_2Me_5^+$, and $P_2Me_6^{+2}$ species were also optimized at the same level of theory, without an experimental starting point. These optimized geometries were then used to obtain theoretical densities for each system. The B3LYP basis set has been shown to provide reliable and consistent results for the interpretation of the electron density in small molecules.[19−21] The evaluation of the topological features of the theoretical electron density were carried out with the Morphy98 software package,[22] while integration of the atomic basins defined by QTAIM[8,9] were obtained using the AIMPAC software package.[23]

Results and Discussion

Structural Details. The hexamethyldiphosphonium ditriflate compound crystallizes in the trigonal space group, *R*-3*m* #166 (Table 1). Figure 1 shows an ORTEP view of the structure, indicating the atom labeling for the asymmetric unit. In the solid state, the P1, S1, and C1 atoms all lie on the same three-fold

TABLE 2: Properties of the Bond Critical Points for Select Chemical Bonds

bond	$\rho_b(\mathbf{r})$ (eÅ^{-3})	$\nabla^2\rho_b(\mathbf{r})$ (eÅ^{-5})	λ_1 (eÅ^{-5})	λ_2 (eÅ^{-5})	λ_3 (eÅ^{-5})	R_{ij} (Å)
P1−X26_P1	1.15	−7.25	−6.32	−6.31	5.38	2.200
2/3-X, 4/3-Y, 1/3-Z						
theory	*0.82*	*−4.45*	*−3.50*	*−3.50*	*2.56*	*2.240*
P1−C2	1.21	−9.85	−7.82	−6.16	4.14	1.785
theory	*1.16*	*−5.75*	*−5.46*	*−5.25*	*4.97*	*1.816*
O1−S1	2.27	−9.92	−19.55	−17.45	27.08	1.447
theory	*1.86*	*19.66*	*−11.08*	*−10.40*	*41.14*	*1.488*
S1−C1	1.55	−13.94	−11.14	−11.08	8.28	1.837
theory	*1.28*	*−8.98*	*−7.82*	*−7.82*	*6.66*	*1.877*
C1−F1	2.08	−27.09	−19.02	−17.66	9.59	1.334
theory	*1.88*	*−6.63*	*−15.66*	*−13.32*	*22.35*	*1.343*

rotation axis. When the operations of the three-fold axis are taken into account, this produces one complete triflate molecule and half the dication. The full structure is then obtained by inversion through a center located at the midpoint of the P−P bond. This geometry results in an ideally staggered conformation of the dication [∠C−P−P−C = 60, 180°].[2] This differs slightly from the optimized gas-phase compound [C_1 point group], which results in a closer interaction between the dication and anions [P···S = 4.060(1) Å (exp) and 3.782 Å (theory)]. These differences result in slight variations in the inter-ion bifurcated C−H···O interactions for the crystalline and gas-phase compounds. Thus, the ideally staggered conformation observed in the crystalline state is not maintained in the gas-phase compound [∠C−P−P−C = −59.94, 60.10, 180°]. However, the optimized isolated gas-phase dication (in the absence of the two triflate counter anions) has a D_3d geometry, consistent with the ideally staggered crystalline geometry.

The internuclear P−P distances in the crystalline [2.200(1) Å] and gas-phase [2.240 Å] structures, both fall within the same range as those of experimentally determined neutral[24] [2.191−2.260 Å], monocationic[25] [2.133−2.307 Å], and dicationic[2] [2.216−2.237 Å] P−P bonds. This seems to indicate that variations in coordination and molecular charge on each phosphorus center play only a small role in the overall P−P internuclear distance.

The internuclear distances can also be used to estimate the bond order for the desired P−P bonds using the Pauling model.[26]

$$n = \exp[-(r - r_o)/a] \quad (1)$$

where r_o is an idealized single P−P internuclear distance [2.256 Å][27] and $a = 0.3$ represents a constant used for any type of covalent bond. Thus, the P−P bond of the dication has a calculated bond order of ∼1.205 (exp) and ∼1.055 (theory). These values are consistent with previous NBO and NLMO calculations [NBO = 0.861, NLMO = 0.953], which indicates the presence of a P−P single bond.[2]

Topological Analysis of Hexamethyldiphosphonium Ditriflate. The geometrical evidence for the hexamethyldiphosphonium dication seems to suggest the presence of a covalent bond between the two adjacent positively charged P atoms. The actual chemical nature of this bond is still somewhat of a mystery,

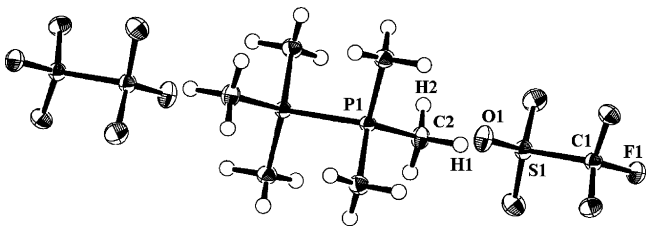

Figure 1. ORTEP view of hexamethyldiphosphonium ditriflate at 123 K with 50% ellipsoid probability for all heavy atoms.

since a large electrostatic repulsion must exist between the two P atoms. A topological and atomic basin analysis provides further insight into the electronic nature of this P−P bond on the basis of its observed and calculated electron densities. Table 2 outlines the relevant topological parameters obtained from the BCP for the symmetrically independent chemical bonds in the title compound.

The chemical bonds in the title compound each possess reasonable bond paths with consistently longer R_{ij} values in the gas-phase compared with the crystalline environment. The calculated R_{ij} values exceed the experimental values by approximately 2%, as found in a previous structural study of diphosphonium dications.[7] The small variations in the R_{ij} values can possibly account for the differences in the experimental and theoretical topological properties of the electron density. The expected covalent bonds (i.e., C−F bonds, etc) each possess $\rho_b(\mathbf{r})$ values consistent with those observed for similar chemical bonds.[28−30] The P−P bond in the theoretical [$\rho_b(\mathbf{r}) = 0.820$ eÅ^{-3}] and experimental [$\rho_b(\mathbf{r}) = 1.150$ eÅ^{-3}] dications both accumulate a significant amount of electron density. These values are considerably larger than those of closed-shell interactions.[31] The $\rho_b(\mathbf{r})$ values for the P−P bonds are comparable to those of other P−X single bonds (X = C, O, and S), which range between 1.107 and 1.336 eÅ^{-3}.[32−34] The accumulation of the electron density in these P−X bonds increases in the following order P−C > P−O > P−S > P−P, which nearly mimic that of single C−X bonds (C−C > C−O > C−S ≥ C−P). However, the more covalent nature of the C−X bonds results in larger $\rho_b(\mathbf{r})$ values than their corresponding P−X analogues. The accumulation of electron density in the P−P bond is significantly less than analogous covalent bonds, which seems to support previous theoretical calculation, that cleavage of the P−P bond is both feasible and thermodynamically supportable.[7]

In charge density studies, the Laplacian ($\nabla^2\rho_b(\mathbf{r})$, eÅ^{-5}) at the BCP represents the sum of the eigenvalues of the Hessian matrix [$\nabla^2\rho_b(\mathbf{r}) = \lambda_1 + \lambda_2 + \lambda_3$] where λ_1, λ_2, and λ_3 represent the curvature of the electron density at the BCP. The first two curvatures (λ_1, λ_2) are perpendicular to the bond path while the third (λ_3) is along the bond path. Therefore, the $\nabla^2\rho_b(\mathbf{r})$ values can be used to measure the charge depletion or concentration along any chemical interaction. The negative $\nabla^2\rho_b(\mathbf{r})$ values associated with the P−P bond [−4.450 (theory) and −7.249 (exp) eÅ^{-5}] indicate that a local charge density concentration is occurring along both the experimental and the theoretical P−P bonds (Figures 2 and 3). This confirms the existence of a covalent bond between the adjacent phosphorus atoms.

The remaining $\nabla^2\rho_b(\mathbf{r})$ values in the title compound each possess large negative values, reflecting their covalent nature. The theoretical S−O bonds are exceptions, since they possess large positive $\nabla^2\rho_b(\mathbf{r})$ values ($\nabla^2\rho_b(\mathbf{r}) = 19.650$ eÅ^{-5}), characteristic of closed-shell interactions. This is a result of

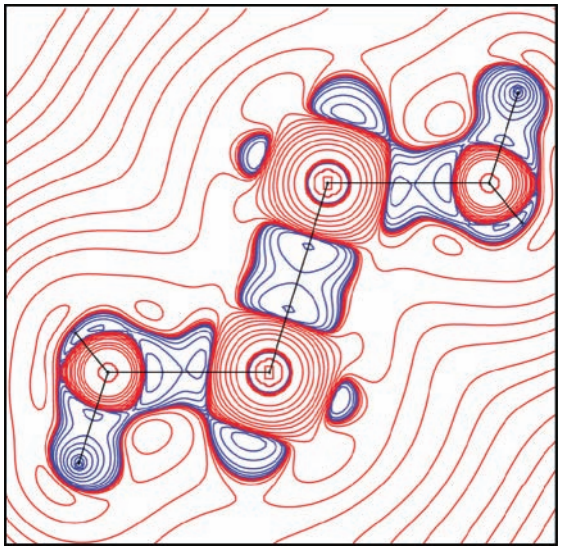

Figure 2. Laplacian distribution along the P−P bond in hexamethyldiphosphonium ditriflate. The contours are drawn at logarithmic intervals in $-\nabla^2\rho_b(\mathbf{r})$, shown in positive (blue) and negative (red) contours. (Note: The Laplacian is generally represented as $-\nabla^2\rho_b(\mathbf{r})$; blue thus indicates an accumulation of electron density.)

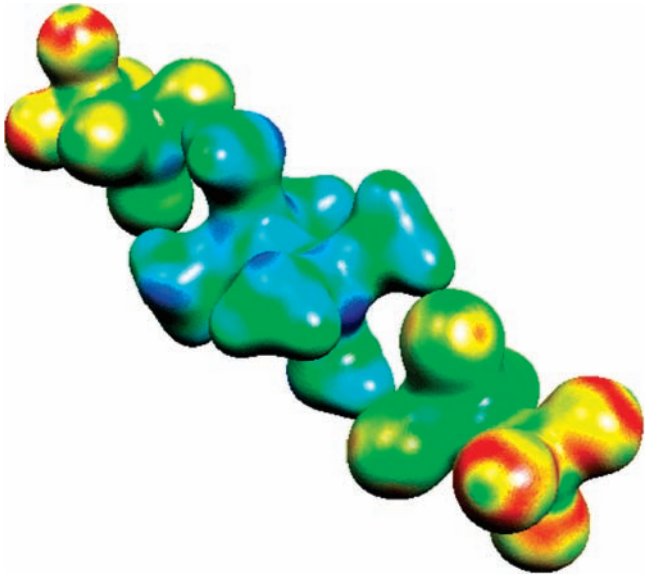

Figure 3. Illustrative plot of the Laplacian mapped onto an isodensity surface [$\rho(\mathbf{r}) = 0.05$ eÅ^{-3}] in the range −0.368 (red) to +0.028 (blue) eÅ^{-5} for hexamethyldiphosphonium ditriflate.

significantly large theoretical λ_3 values, which represent the curvature at BCP along the bond paths. This has previously been observed for SO_3 groups in both famotidine and taurine.[35,36] Where the positive values can be attributed to the BCP location, which can be found in the vicinity of the positive $\nabla^2\rho_b(\mathbf{r})$ region surrounding the S atom [S···BCP = 0.577 Å]. This seems to highlight the polar nature of the $S^{\delta+}-O^{\delta-}$ bonds, where the BCP is pushed toward the least electronegative atom. In the experimental S−O bonds, the S···BCP distance [0.595 Å] lies slightly further away from the S atom, which results in negative $\nabla^2\rho_b(\mathbf{r})$ values. The large difference between the experimental and the theoretical $\nabla^2\rho_b(\mathbf{r})$ values can therefore be attributed to small differences in the position of the BCP, where the $\nabla^2\rho_b(\mathbf{r})$ surface is rapidly changing in this internuclear region.[35]

The formation of chemical bonds results in distortions in spherical charge distribution, which leads to the local maxima and minima in the valence shell of charge concentration

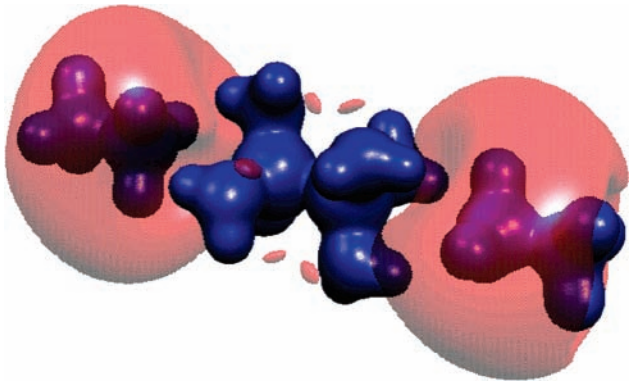

Figure 4. Molecular electrostatic potentials. The potential of +0.1 eÅ^{-1} is shown as the blue isosurface, while the potential of −0.1 eÅ^{-1} is shown as the red isosurface.

SCHEME 2: Addition−Elimination Mechanism

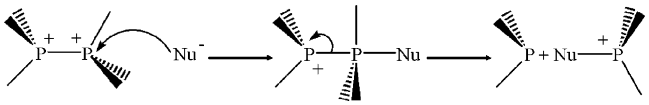

(VSCC).[37] The centers of charge concentration (maxima) correspond to sites susceptible to electrophilic attack, while those of charge depletion (minima) serve as sites for nucleophilic attack. The direction of the nucleophilic attack is always determined by the largest "hole" (charge depletion) in the $\nabla^2\rho_b(\mathbf{r})$ surface.[37] In the title compound, the Laplacian values mapped onto a $\rho(\mathbf{r}) = 0.05$ eÅ^{-3} isodensity surface (Figure 3), clearly illustrates a region of charge depletion located directly opposite the P−P bond. This supports the directional approach of a nucleophile in the addition−elimination mechanism previously proposed for 1,2-diphosphonium dications (Scheme 2).[3,38]

The reaction of 1,2-diphosphonium dications can result in either homolytic cleavage of the P−P bond or heterolytic cleavage of the P−C bonds.[7] However, slightly larger $\rho_b(\mathbf{r})$ and $\nabla^2\rho_b(\mathbf{r})$ values for the P−C bonds seem to indicate that homolytic cleavage of the P−P bond would be more favorable than heterolytic cleavage of the P−C bonds. This supports previous reactions of *in situ* prepared 1,2-diphosphonium dications through electrochemical oxidation with a variety of nucleophiles (examples A−C), which consistently show cleavage of the P−P bond.[39]

$$R_3P^+ - P^+R_3 + EtSSEt \rightarrow 2R_3P(SEt)^+ \quad \text{(A)}$$

$$R_3P^+ - P^+R_3 + Et_2NH \rightarrow R_3P(NEt_2)^+ + R_3PH^+ \quad \text{(B)}$$

$$R_3P^+ - P^+R_3 + F^- \rightarrow R_3PF - P^+R_3 + F^- \rightarrow R_3PF_2 + PR_3 \quad \text{(C)}$$

Topological Analysis of the Weak Interactions. The experimental and theoretical hexamethyldiphosphonium ditriflate geometries result in the formation of several unique types of weak interactions (C−H···O, C−H···F, and C−F···F−C). These interactions have all been characterized as weak hydrogen bonds (HB) or van der Waals interactions (VDW) based on the first four criteria for hydrogen bonding proposed by Koch and Popelier.[40] The relevant topological properties associated with each of these interactions are listed in Table 3.

In the crystalline state, the title compound forms a total of six symmetrically independent interactions (four C−H···O, one C−H···F, and one C−F···F−C). The molecular electrostatic potential map (Figure 4), illustrates the preferred binding sites

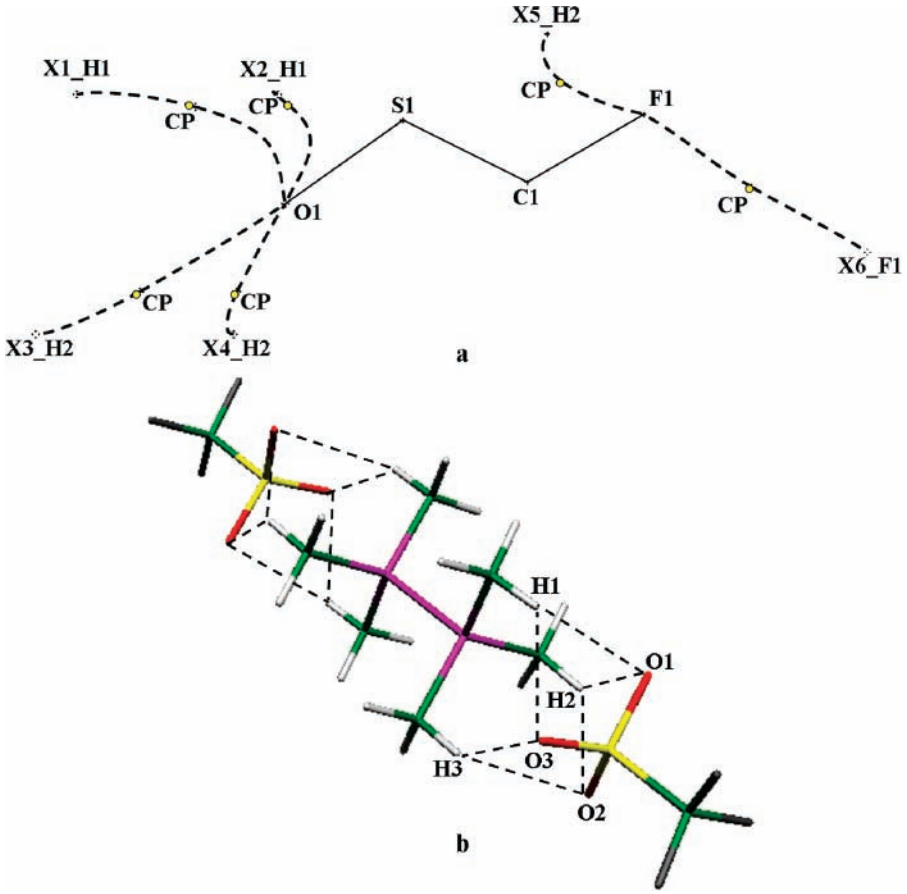

Figure 5. (a) Bond path character, showing the BCP locations along all three types of weak interactions. The symmetry codes are the same as those listed in Table 3. (b) Structural diagram of hexamethyldiphosphonium ditriflate illustrating the gas-phase bifurcated C−H···O hydrogen bonds (dashed lines).

TABLE 3: Properties of the Bond Critical Points for the Symmetrically Independent Weak Interactions

bond	$\rho_b(\mathbf{r})$ (eÅ^{-3})	$\nabla^2\rho_b(\mathbf{r})$ (eÅ^{-5})	R_{ij} (Å)	$\Delta r_H + \Delta r_B$ (Å)	$\Delta r_H - \Delta r_B$ (Å)	bond energies (kJ/mol bohr^3)	hydrogen bond
Experimental:							
O1···X1_H1,$^{1-Y,1+X-Y,+Z}$	0.04	0.58	2.771	−0.031	0.161	−4.229	VDW
O1···X2_H1,$^{-X+Y,1-X,+Z}$	0.04	0.57	2.784	−0.044	0.173	−4.193	VDW
O1···X3_H2,$^{-2/3+Y,-1/3-X+Y,2/3-Z}$	0.04	0.72	2.551	0.189	0.100	−4.775	HB
O1···X4_H2,$^{1/3-X,-1/3-X+Y,2/3-Z}$	0.04	0.72	2.552	0.188	0.100	−4.771	HB
F1···X5_H2,$^{-1/3-X+Y,4/3-X,1/3+Z}$	0.04	0.73	2.569	0.101	0.053	−4.978	HB
F1···X6_F1,$^{-1/3+Y,1/3-X+Y,4/3-Z}$	0.02	0.43	3.119	−0.179	0.006	−2.595	VDW
Theoretical:							
O1···H1	0.07	0.86	2.482	0.259	0.180	−7.587	HB
O3···H1	0.09	1.04	2.317	0.423	0.175	−10.727	HB
O1···H2	0.07	0.86	2.488	0.252	0.179	−7.485	HB
O2···H2	0.09	1.03	2.319	0.421	0.175	−10.681	HB
O2···H3	0.07	0.86	2.482	0.258	0.179	−7.583	HB
O3···H3	0.09	1.03	2.321	0.420	0.175	−10.644	HB

for these weak interactions. The strength of an intermolecular interaction can be estimated from the potential energy density as follows:[41,42]

$$\text{Bond Energy} = 1/2\ V(\mathbf{r}) \qquad (2)$$

The strengths of these weak interactions range from −2.595 to −4.978 kJ/mol bohr^3 and increase in the following order C−F···F−C_{VDW} < C−H···O_{VDW} < C−H···O_{HB} < C−H···F_{HB}. The lack of symmetry related molecules in the optimized gas-phase compound results in only C−H···O HBs, which are approximately twice as strong as any of the crystalline interactions [−7.485 to −10.727 kJ/mol bohr^3]. This can be attributed to the shorter R_{ij} values, which arise because of a closer cation-to-anion distance. Figure 5a, illustrates all of the rational bond paths and BCPs for the symmetrically independent interactions in the crystalline state. It should be remembered that the anions contain only one unique F and O atom. Figure 5b shows the birfucated C−H···O hydrogen-bonding network present in the gas-phase structure.

The experimental and the theoretical C−H···O interactions each form bifurcated interactions to every O atom of the triflate anions. The experimental C−H···O interactions show only slight differences in the bond energies associated with each interaction involved in the bifurcation. However, the theoretical bifurcated

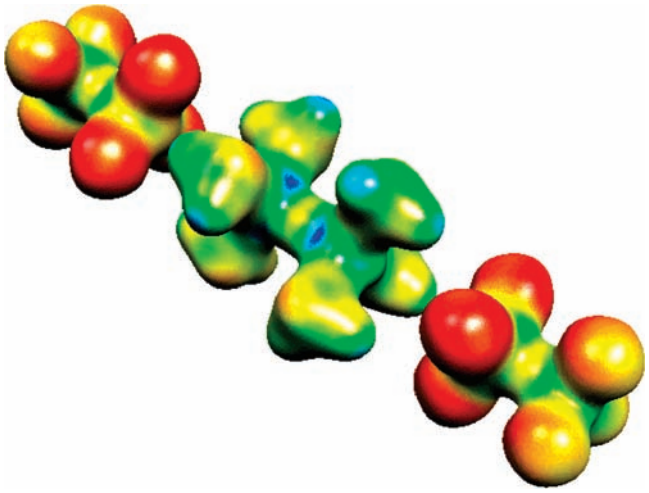

Figure 6. Illustrative plot of the electrostatic potential mapped onto an isodensity surface [$\rho(\mathbf{r}) = 0.05$ eÅ^{-3}] in the range -0.139 (red) to $+0.548$ (blue) eÅ^{-1} for hexamethyldiphosphonium ditriflate.

TABLE 4: Atomic Charges

atom	experimental q (au)	theoretical q (au)
P1	1.80	2.02
S1	3.36	3.22
$C1_{triflate}$	1.21	1.71
$C2_{methyl}$	−0.60	−0.63
O1	−1.29	−1.34
F1	−0.54	−0.62
H1	0.06	0.18
H2	0.12	0.05
H3		0.05
overall	0.04	0.00

TABLE 5: Properties of the Bond Critical Points for the P−P Bond in P_2Me_4, $P_2Me_5^+$, $P_2Me_6^{+2}$

isolated molecule	$\rho_b(\mathbf{r})$ (eÅ^{-3})	$\nabla^2\rho_b(\mathbf{r})$ (eÅ^{-5})	R_{ij} (Å)	bond energies (kJ/mol bohr^3)
P_2Me_4	0.76	−3.40	2.253	−183.296
$P_2Me_5^+$	0.78	−3.78	2.232	−188.238
$P_2Me_6^{+2}$	0.78	−3.99	2.264	−190.078

C−H···O HBs possess one interaction that is significantly stronger than the other. In the (theoretical) gas-phase, the C−H···O interactions represent weak HBs. However, longer cation-to-anion distances in the crystalline state result in one pair of weak C−H···O HBs and another pair of C−H···O VDW interactions.

The weak HBs and VDW interactions each experience a significant accumulation of electron density at the BCP. In the case of the crystalline C−H···O interactions, no difference is observed between those classified as weak hydrogen bonds and those of the VDW interactions. However, the $\nabla^2\rho_b(\mathbf{r})$ values for these interactions show a distinct difference between the VDW C−H···O interactions [$\sim$0.5 eÅ^{-5}] and the weak C−H···O HBs [$\sim$0.7 eÅ^{-5}]. This seems to indicate that the Laplacian parameter represents a better measure of hydrogen-bonding character than the actual accumulation of electron density. The weak HBs each experience a significant amount of mutual penetration ($\Delta r_A + \Delta r_B$) between the donor and the acceptor atoms, while those of the VDW interactions are not mutually penetrated. The amount of mutual penetration mimics the overall bond energies associated with these interactions.

In the crystalline state, the absence of strong HBs results in the dication forming six unique weak HBs and eight VDW interactions for a total of 42 weak interactions (18 weak HBs and 24 VDW interactions). These interactions [−2.595 to −4.978 kJ/mol bohr^3], with a cumulative bond strength of $\sim$150 kJ/mol bohr^3, must play an important role in stabilizing the crystal structure of hexamethyldiphosphonium ditriflate. This is also the case in the gas-phase compound, where a total of 12 weak C−H···O HBs contribute to the overall stability of the compound.

Atomic Charges. The experimental and theoretical atomic charges obtained from integrations over the atomic basins for each atom provide important information about the charge localization in the hexamethyldiphosphonium ditriflate structure (Table 4). The atomic charges for each P atom are significantly positive, while each methyl group carries a small negative charge [−0.29 au (exp) and −0.36 au (theory)]. This provides an overall PMe_3 charge of +0.94 au (exp) and +0.94 au (theory), which indicates that the positive charges associated with the dication are primarily localized on each P atom. The molecular electrostatic potential mapped onto a $\rho(\mathbf{r}) = 0.05$ eÅ^{-3} isodensity surface (Figure 6) clearly highlights this localization. The localization of nearly all of the positive charge on the two P atoms suggests that a strong electrostatic repulsion must exist between these two heteroatoms, despite the covalent nature of the P−P bond.

The S and C atoms of the triflate anions each possess significant positive charges, while the O and F atoms carry the negative charge. The overall charges associated with the SO_3 and CF_3 groups are −0.52 au (exp)/−0.79 au (theory) and −0.42 au (exp)/−0.15 au (theory), respectively. This shows that the experimental and theoretical anions possess different localizations of the negative charge. In the gas phase, the negative charge is almost exclusively localized on the SO_3 groups, and in the crystalline state, it is nearly evenly distributed between the SO_3 and the CF_3 groups (Figure 6). The distribution of the charge by weak C−H···F, C−F···F−C interactions, and weaker C−H···O interactions in the crystalline state can possibly account for this difference.

Progression of the P−P Bond. The topological and atomic basin properties associated with the neutral (P_2Me_4) and monocationic ($P_2Me_5^+$) species involved in the synthesis of the title compound (dication ($P_2Me_6^{+2}$)) have also been determined to examine the successive changes in the P−P bond (Figure 7). The topological properties associated with the P−P bond for each of these chemical species are listed in Table 5.

The monocation possesses the shortest P−P interaction of the three molecules, since the volumes associated with each P atom [$V = 72.03$ (PMe_3) and 144.76 (PMe_2) au] are significantly smaller than those in the neutral molecule [$V = 155.28$ (PMe_2) au]. This can be attributed to the positive charge associated with the monocation [$q = 0.65$ (PMe_3) and 0.35 (PMe_2) au], which reduces the size of these atoms. The dication results in the longest P−P interaction, despite the small volumes associated with each P atom [$V = 71.08$ (PMe_3) au]. This can be attributed to the large electrostatic repulsion that must exist between the two P atoms (the neutral molecule experiences no electrostatic repulsion and the monocation experiences less electrostatic repulsion compared to the dication).

A general increase from neutral to dicationic species is observed for the $\rho_b(\mathbf{r})$ values. This indicates that the dication accumulates more electron density than the neutral or monocationic species, despite experiencing a strong electrostatic repulsion between the two heteroatoms. A similar trend is observed for the degree of covalency, as measured by the $\nabla^2\rho_b$-

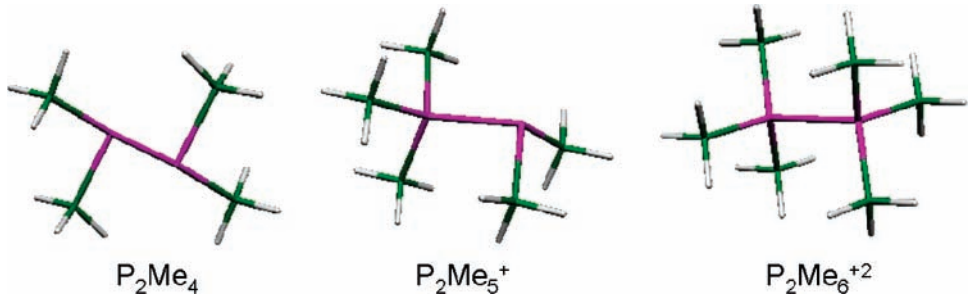

Figure 7. B3LYP/6-31++G(d,p) level optimized structures of P_2Me_4, $P_2Me_5^+$, and $P_2Me_6^{+2}$

(**r**) values. These parameters indicate that the P−P bond increases in strength as the coordination and charge of the P atoms increases. It would appear that the electrostatic repulsion does little to hinder the formation of a stronger, more covalent P−P bond in the dication.

Conclusions

Investigation of the experimental and theoretical electron densities of hexamethyldiphosphonium ditriflate has led to a thorough understanding of the electronic structure of this 1,2-dication. The accumulation of electron density along the P−P bond shows that cleavage of this bond is feasible when reacted with nucleophiles. Through analysis of the $\nabla^2\rho_b(\mathbf{r})$ values, the P−P bond has been shown to be covalent in nature. This parameter has also allowed for an examination of the reactivity of this compound, where nucleophilic attack can occur directly opposite the P−P bond. In the absence of strong hydrogen bonds, the hexamethyldiphosphium ditriflate salt forms a large number of weak interactions (C−H···O, C−H···F, and C−F···F−C), which contribute to the stabilization of the crystalline structure. In the gas phase, the compound can only form weak C−H···O hydrogen bonds between the dication and the triflate anions. The experimental and theoretical atomic charges show a localization of the positive charge on each P atom of the dication. This indicates that a large electrostatic repulsion must exist between these two heteroatoms. The charges associated with the anions show significant differences between experiment and theory. Where experimentally the negative charge is nearly equally distributed on the SO_3 and CF_3 groups, theoretically, it is primarily localized on the SO_3 portion of the anion. An investigation of the isolated P_2Me_4, $P_2Me_5^+$, and $P_2Me_6^{+2}$ species has shown that the dication P−P bond is stronger than those of the corresponding neutral and monocationic species. This is also reflected in the topological features of the electron density, where the P−P bond accumulates the greatest amount of electron density and is the most covalent in nature.

Acknowledgment. Dedicated to Professor Keith Prout (Oxford, U.K.) 1934−2007 who nurtured many chemical crystallographers. We thank the Natural Science and Engineering Research Council of Canada and the Alexander von Humboldt Foundation (Feodor Lynen Return Fellowship for J.J.W.) for financial support. T.S.C. acknowledges 43 years of chemical discussions, crystallographic advice, and structural wisdom provided by Keith Prout (1934−2007). We would also like to thank Dr. K. N. Robertson for insightful discussions.

Supporting Information Available: Residual maps and all of the crystallographic information files. This material is available free of charge via the Internet at http://pubs.acs.org.

References and Notes

(1) Dillon, K. B.; Mathey, F.; Nixon, J. F. *Phosphorus: The Carbon Copy*; John Wiley & Sons: New York, 1997.
(2) Weigand, J. J.; Riegel, S. D.; Burford, N.; Decken, A. *J. Am. Chem. Soc.* **2007**, 129(25), 7969−7976.
(3) Nenajdenko, V. G.; Shevchenko, N. E.; Balenkova, E. S. *Chem. Rev.* **2003**, 103, 229−282.
(4) Schomburg, D.; Bettermann, G.; Ernst, L.; Schmutzler, R. *Angew. Chem., Int. Ed. Engl.* **1985**, *24*, 975−976.
(5) Alder, R. W.; Ganter, C.; Harris, C. J.; Orpen, A. G. *Chem. Commun.* **1992**, 1172−1174.
(6) Kilian, P.; Slawin, A. M. Z.; Woollins, J. D. *Dalton Trans.* **2006**, 2175−2183.
(7) Zagumennov, V. A.; Vedornikov, A. N.; Nikitin, E. V.; Solomonov, B. N. *Zh. Obshch. Khim.* **2003**, *73*, 921−927.
(8) Bader, R. F. W. *Atoms in Molecules: A Quantum Theory*; Oxford University Press: Oxford, U.K., 1990.
(9) Popelier, P. L. A. *Atoms in Molecules: An Introduction*; Prentice Hall: London, U.K., 2000.
(10) Thorne, R. E.; Stum, Z.; Kmetko, J.; O'Neill, K.; Gillilan, R. *J. Appl. Cryst.* **2003**, *36*, 1455−1460.
(11) (a) Rigaku Corporation, *CrystalClear*. CrystalClear Software User's Guide, Molecular Structure Corporation, 1999. (b) Plugrath, J. W. *Acta Cryst.* **1999**, *D55*, 1718−1725.
(12) Rigaku and Rigaku/MSC; *CrystalStructure. Version 3.6.0*; Rigaku and Rigaku/MSC, The Woodlands: Texas, 2000−2004.
(13) Coppens, P. *X-Ray Charge Densities and Chemical Bonding*; Oxford University Press, Inc.: New York, 1997.
(14) Volkov, A.; Macchi, P.; Farrugia, L. J.; Gatti, C.; Mallinson, P.; Richter, T.; Koritsanszky, T. *XD2006, A Computer Program Package for Multipole Refinement, Topological Analysis of Charge Densities and Evaluation of Intermolecular Energies from Experimental and Theoretical Structure Factors*; 2006.
(15) Su, Z.; Coppens, P. *Acta Cryst.* **1998**, *A54*, 646.
(16) Macchi, P.; Coppens, P. *Acta Cryst.* **2001**, *A57*, 656.
(17) Allen, F. H. *Acta Cryst.* **1986**, *B42*, 512−522.
(18) MOLEKEL is a free graphics program available from http://www.cscs.ch/molekel/.
(19) Wolstenholme, D. J.; Matta, C. F.; Cameron, T. S. *J. Phys. Chem. A* **2007**, *111*, 8803−8813.
(20) Oddershede, J.; Larsen, S. *J. Phys. Chem. A* **2004**, *108*, 1057−1063.
(21) Munshi, P.; Row, T. N. G. *J. Phys. Chem. A* **2005**, *109*, 659−672.
(22) *MORPHY98*; a program written by P.L.A. Popelier with contribution from R.G.A. Bone, UMIST: Manchester, England, 1998.
(23) Bader, R. F. W. *AIMPAC*; http://www.chemistry.mcmaster.ca/aimpac/.
(24) (a) Baxter, S. G.; Cowley, A. H.; Davis, R. E.; Riley, P. E. *J. Am. Chem. Soc.* **1981**, *103*(7), 1699−1702. (b) Fritz, G.; Matem, E.; Krautscheid, H.; Ahlrichs, R.; Olkowska, J. W.; Pikies, J. *Z. Anorg. Allg. Chem.* **1999**, *625*, 1604−1607. (c) Dashti-Mommertz, A.; Neumuller, B. *Z. Anorg. Allg. Chem.* **1999**, *625*, 954−960. (d) Hinchley, S. L.; Robertson, H. E.; Borisenko, K. B.; Turner, A. R.; Johnston, B. F.; Rankin, D. W. H.; Ahmadian, M.; Jones, J. N.; Cowley, A. H. *Dalton Trans.* **2004**, 2469−2476. (e) Burford, N.; Ragogna, P. J.; McDonald, R.; Ferguson, M. J. *J. Am. Chem. Soc.* **2003**, *125*, 14404−14410.
(25) (a) Abrams, M. B.; Scott, B. L.; Baker, R. T. *Organometallics* **2000**, *19*, 4944−4956. (b) Romanenko, V. D.; Rudzevich, V. L.; Rusanov, E. B.; Chernega, A. N.; Senio, A.; Sotiropoulos, J. M.; Pflister-Guillouzo; Sanchez, M. *Chem. Commun.* **1995**, 1383−1385. (c) Schmidpeter, A.; Lochschmidt, S.; Karaghiosoff, K.; Sheldrick, W. S. *J. Chem. Soc., Chem. Commun.* **1985**, 1447−1448. (d) David, G.; Niecke, E.; Nieger, M.; Radseck, J.; Schoeller, W. W. *J. Am. Chem. Soc.* **1994**, *116*, 2191−2192. (e) Burford, N.; Ragogna, P. J.; McDonald, R.; Ferguson, M. J. *Chem. Commun.* **2003**, 2066−2067.
(26) Pauling, L. *The Nature of the Chemical Bond*; Cornell University Press: Ithaca, NY, 1960.

(27) *International Tables for Crystallography*; Mathematical, Physical and Chemical Tables, Volume C; Wilson, A. J. C., Ed.; Kluwer Academic Publishers: Norwell, MA, 1992.

(28) Wolstenholme D.; Aquino, M. A. S.; Cameron, T. S.; Ferrara, J. D.; Robertson, K. N. *Can. J. Chem.* **2006**, *84*, 804−811.

(29) Hibbs, D. E.; Austin-Woods, C. J.; Platts, J. A.; Overgaard, J.; Turner, P. *Chem. Eur. J.* **2003**, *9* (5), 1075−1084.

(30) Lentz, D.; Patzschke, M.; Bach, A.; Scheins, S.; Luger, P. *Org. Biomol. Chem.* **2003**, *1*, 409−414.

(31) Lee, C. R.; Wang, C. C.; Chen, K. C.; Lee, G. H.; Wang, Y. *J. Phys. Chem.* A **1999**, *103*, 156−165.

(32) Lledos, A.; Carbo, J. J.; Urriolabeitia, E. P. *Inorg. Chem.* **2001**, *40*, 4913−4917.

(33) Kocher, N.; Leusser, D.; Murso, A.; Stalke, D. *Chem. Eur. J.* **2004**, *10*, 3622−3631.

(34) Kuivalainen, T.; El-Bahraoui, J.; Uggla, R.; Kostiainen, R.; Sundberg, M. R. *J. Am. Chem. Soc.* **2000**, *122*, 8073−8074.

(35) Hibbs, D. E.; Austin-Woods, C. J.; Platts, J. A.; Overgaard, J.; Turner, P. *Chem. Eur. J.* **2003**, *9* (5), 1075−1084.

(36) Overgaard, J.; Hibbs, D. E. *Acta Cryst.* **2004**, *A60*, 480−487.

(37) Shi, Z.; Boyd, R. J. *J. Phys. Chem.* **1991**, *95*, 4698−4701.

(38) Romanhin, A. S.; Palutin, F. M.; Nikitin, E. V. *Zh. Obshch. Khim.* **1996**, *66*, 930−935.

(39) Nikitin, E. V.; Romakhin, A. S.; Zagumennov, V. A.; Babkin, Y. A. *Elektrochim. Acta* **1997**, *42* (13−14), 2217−2224.

(40) Koch U.; Popelier P. L. A. *J. Phys. Chem.* **1995**, *99*, 9747−9754.

(41) Abramov, Y. A. *Acta Cryst.* **1997**, *A53*, 264−272.

(42) Espinosa, E.; Alkorta, I.; Elguero, J.; Molins, E. *J. Chem. Phys.* **2002**, *117*, *12*, 5529−5542.